

UNIVERSIDAD SAN FRANCISCO DE QUITO USFQ

COLEGIO DE CIENCIAS E INGENIERÍAS

**A geometry-based algorithm for cloning real  
grains 2.0**

Proyecto de Investigación

*David Alberto Medina Alvarez*

Matemáticas

Trabajo de titulación presentado como requisito para la obtención del título  
de  
Licenciatura en Matemáticas

Quito, 24 de mayo de 2018

UNIVERSIDAD SAN FRANCISCO DE QUITO USFQ

COLEGIO DE CIENCIAS E INGENIERÍAS

HOJA DE CALIFICACIÓN

DE TRABAJO DE TITULACIÓN

**A geometry-based algorithm for cloning real  
grains 2.0**

*David Alberto Medina Alvarez*

Calificación:

Nombre del Profesor, Título académico: Alex X. Jerves Ph.D.

Nombre de la Directora del Departamento de Matemáticas, Título  
académico: Andrea T. Moreira Ph.D.

Firma del profesor: \_\_\_\_\_

Firma de la Dir. del Departamento: \_\_\_\_\_

Quito, 24 de mayo de 2018

## Derechos de Autor

Por medio del presente documento certifico que he leído todas las Políticas y Manuales de la Universidad San Francisco de Quito USFQ, incluyendo la Política de Propiedad Intelectual USFQ, y estoy de acuerdo con su contenido, por lo que los derechos de propiedad intelectual del presente trabajo quedan sujetos a lo dispuesto en esas Políticas.

Asimismo, autorizo a la USFQ para que realice la digitalización y publicación de este trabajo en el repositorio virtual, de conformidad a lo dispuesto en el Art. 144 de la Ley Orgánica de Educación Superior.

Firma del Estudiante: \_\_\_\_\_  
Nombres y Apellidos: David Alberto Medina Alvarez  
Código: 00114619  
Cédula de Identidad: 172295889-7  
Lugar y Fecha: Quito, mayo de 2018

## Resumen

Presentamos una versión mejorada de un algoritmo computacional que “clona”/genera un número arbitrario de nuevos granos digitales de una muestra real digitalizada de material granular. Nuestro algoritmo mejorado produce granos “clonados” que aproximan con más precisión las características morfológicas mostradas por sus padres. Ahora, los granos “clonados” también fueron incluidas en una simulación del método de elementos discretos de una prueba tri-axial y mostraron un comportamiento mecánico similar comparado con el mostrado por la muestra original (padres). Así, el presente trabajo esta dividido en cuatro partes. Primero, nosotros calculamos las funciones de densidad de probabilidad multivariantes de las parámetros morfológicos de los padres (ADN morfológico), es decir, relación de aspecto, redondez, relación volumen-superficie y diámetro del grano. Segundo, una mejorada, ahora paralelizada y anada versión del algoritmo estocástico geométrico de clonación [13], el cual está basado en las distribuciones multivariantes antes mencionadas, y que, de la misma manera, introduce un proceso de muestro mejorado de radios, así como también una prueba de control de calidad nuevo basado en la relación volumen-radio es discutido. Tercero, el ADN morfológico de los granos (es decir, relación de aspecto, redondez, relación volumen-superficie y diámetro del grano) es también extraído de los nuevos granos clonados y comparado al obtenido de la muestra padre. Cuarto, los clones y padres son sometidos a una prueba de compresión tri-axial usando el esquema de Elementos Discretos (3DLS-DEM) con Level Sets (LS), y luego, comparados en términos de su respuesta mecánica. Finalmente, el error de los “clones” en morfología y comportamiento mecánico es analizado y discutido para mejoras futuras.

---

Palabras clave: material granular ; parámetros morfológicos ; level sets ; Monte-Carlo multivariable ; método de elementos discretos ; clones

## Abstract

We introduce an improved version of a computational algorithm that “clones”/generates an arbitrary number of new digital grains from a real sample of real digitalized granular material. Our improved algorithm produces “cloned” grains that more accurately approach the morphological features displayed by their parents. Now, the “cloned” grains were also included in a Discrete Element Method simulation of a tri-axial test and showed similar mechanical behavior compared to the displayed by the original (parent) sample. Thus, the present work is divided in four parts. First, we compute multivariable probability density functions (PDF) from the parents’ morphological parameters (morphological DNA), i.e., aspect ratio, roundness, volume-surface ratio, and particle diameter. Second, an improved, now parallelized and better tuned version of the Geometric Stochastic Cloning (GSC) algorithm [13], which is based on the aforementioned multivariable distributions, and that, in the same way, introduces an enhanced radii sampling process, as well as a new quality control test based on the volume-surface ratio is discussed. Third, morphological DNA of the grains (i.e., aspect ratio, roundness, volume-surface ratio and particle diameter) is also extracted from the new “cloned” grains and compared to the one obtained from the parent sample. Fourth, clones and parents are subjected to a tri-axial compression tests using a Level Set (LS) in Discrete Element scheme (3DLS-DEM), and then, compared in terms of their mechanical response. Finally, the error of the “clones” in the morphology and mechanical behavior is analyzed and discussed for future improvements.

---

Keywords: granular materials ; morphological parameters ; level sets ; multivariable Monte-Carlo ; discrete element method ; clones

# Contents

Derechos de Autor	3
Resumen	4
Abstract	5
<b>1 Introduction</b>	<b>10</b>
<b>2 GSC algorithm improvements</b>	<b>13</b>
2.1 Multivariable distributions . . . . .	13
2.2 Multivariable Monte Carlo method . . . . .	14
2.3 Radii sampling . . . . .	15
2.4 Quality control . . . . .	16
2.5 Parallelization and optimization . . . . .	17
<b>3 Algorithm calibration</b>	<b>18</b>
<b>4 Morphological matching</b>	<b>19</b>
4.1 Errors . . . . .	22
4.2 Results . . . . .	23
<b>5 Mechanical matching</b>	<b>25</b>
<b>6 Further improvements</b>	<b>29</b>
<b>7 Conclusions</b>	<b>30</b>
<b>8 Acknowledgements</b>	<b>31</b>
References	32

## List of Tables

1	Morphological parameter's correlation matrix. . . . .	13
2	Node's correlation for a sampled point in the mesh. . . . .	15
3	Parameters of the different versions of the algorithm used in the calibration . . . . .	19
4	Mean error in percentage for each version of the algorithm and each morphological property . . . . .	23
5	Standard deviation error in percentage for each version of the algorithm and each morphological property. . . . .	23
6	Technical characteristics of the computers used to generate a clones sample of 3554. . . . .	24
7	Values of parameters used in simulation of membrane used in the tri-axial tests for the parents and clones . . . . .	25
8	Parents and clones tri-axial test initial conditions after isotropic compression. . . . .	25
9	Error in the tri-axial test initial conditions of clones with respect to parents after isotropic compression. . . . .	26
10	Tri-axial test results for parents and clones with samples of 1000 grains each. In this table, the error has been computed for each parameter and with respect to the parents results. . . . .	28

## List of Figures

1	Cloning's process and mechanical test: a small sample of real soil is extracted and then 3DXRCT scanning is performed on it to obtain level set representations of each grain of the real sample. Then, the grains morphological features are extracted (morphological DNA). This DNA is used to generate multivariable probability density distributions from where data is sampled using a multivariable Monte Carlo scheme. Thus, an embryo (equivalent ellipsoid) is generated by sampling from the parents sample morphological DNA and radii distributions. Finally, a quality control is performed and the embryo is included in a pool new cloned grains that is used for simulation by means of a discrete element scheme (3D LS-DEM). . . . .	11
2	The obtention of multivariable distributions from the morphological DNA. For instance, with two variables (minimum principal direction and volume-surface ratio or aspect ratio) it is possible to generate a two-variable histogram that then, by mens of cubic interpolation, is turned into a two-variable probability density function. . .	14
3	a) For a given mesh point (i,j) of the embryo's spherical mesh with corresponding radii distribution (figure b) color cyan) obtained from the parent's radii values at the same coordinates than those of the mesh point (i,j), and neighboring points on the embryo's spherical. b) Green histogram displays the distribution of radii of regolith simulant for the mesh point (i+1,j), blue histogram for the point (i,j), purple for (i,j+1), orange the point (i,j-1), yellow for (i-1,j) which is on the back. . . . .	15
4	From left to right: an embryo resulting from the radii sampling method of version 1.0, and an embryo resulting from the improved radii sampling, both generated from a pool of 2769 parents. . . . .	16
5	Grain's acceptance rate with respect to error tolerance using sets of 50 grains. . . . .	17
6	Embryo's higher spherical mesh resolution. Left: spherical mesh of $16 \times (8 + \text{poles})$ . Right: spherical mesh of $28 \times (18 + \text{poles})$ . . . . .	18
7	Left: grain's level set grid made of $30 \times 30 \times 30$ points. Right: same grain with a level set grid of $45 \times 45 \times 45$ . . . . .	19
8	Aspect ratio distributions calculated for the clones and parents . . . . .	21



9	Roundness distributions obtained from parents and clones . . . . .	21
10	Grain's diameter distribution calculated for the clones and parents . . . . .	21
11	Volume to surface ratio computed for parents and clones . . . . .	22
12	percentage of grains passing versus log of grain's diameter corresponding to last figure	22
13	Five random sampled regolith simulant parents and clones for visual inspection and comparison. . . . .	24
14	Samples of 1000 grains after hydrostatic compression of a) parents b) clones. . . . .	27
15	Friction angle mobilization versus axial strain from the samples of parents and clones made of 1000 grains each, and undergoing tri-axial compression. Here, red line corresponds to parents and blue line to clones. . . . .	27
16	Final configuration after the tri-axial compression tests have finished with a total axial deformation of 20% a) parents and b) clones. . . . .	28

# 1 Introduction

The development of the discrete element method (DEM) in computational geo-physics and civil engineering played a fundamental role when it comes to understand the macroscopic behavior of granular materials [1, 2] in terms of micro and meso- scale mechanisms [4–7]. Since DEM was first introduced, particle interactions have been modeled using planes [8], non-uniform rational B-splines (NURBS) and now, Level Sets (LS) to make faster calculations due it’s lower computational cost [16, 28]. Level sets are functions which are easy to use for the representation of surfaces, allowing for the simplification of calculations and therefore, minimizing computational cost. In the same way, the inclusion of arbitrary shapes in DEM simulations has been of key importance to accurately reproduce the physics involved in the bulk behavior of granular materials [3, 8–11]. With this aim, several DEM schemes have been used to improve shape effects capture. Thus, polygonal shapes, spheres and dumping are among the most popular nowadays [9–11]. In the last twenty years, 3D X-ray Computed Tomography scanning (3DXRCT) has made possible to recover real shapes of granular materials [26, 27] such as Hostun sand [21] with very high detail and include them into DEM simulations [15, 20]. However, costly equipment and specialized personal is needed to perform this 3D X-ray CT scans. In addition, the size of the scanned samples is small (a few thousand grains) compared to the amount and the size of the material required to reproduce macroscopic/engineering behavior.

The ultimate goal of this study is to generate new “cloned” grains, that accurately capture and reproduced the morphological features of any given sample of real granular materials, with the aim of using them as part of DEM based engineering-scale simulations overcoming sample size constrains inherent to 3DXRCT scanning processes. This, together with recent works [21] that have shown the importance of shape when not only qualitatively, but quantitatively matching the mechanical behavior of real granular materials, promise to become a powerful tool to simulate engineering scale processes involving granular materials.

Thus, to ameliorate the high cost, time consuming and size constraints of 3DXRCT scanning, a first computational algorithm was developed to obtain morphological features from a sample of real grains, (i.e., aspect ratio, principal geometric directions, roundness and spherical radius)[13]. This first algorithm successfully reached its goal of generating new grains (clones) similar to ones from a

parent sample. First, it was assumed that the morphological variables were uncorrelated. However, this first version of the cloning algorithm showed some limitations and problems which are overcome by the algorithm's version now introduced by this work. Here, we show that these variables are, in fact, correlated, and therefore, the former single variable sampling scheme was substituted by a multivariable sampling method. Similarly, the radii sampling method in the generation of the cloned grain's embryo assumed that there were no correlation between the values of radius of neighboring points on the grain's surface. This has been enhanced by including the aforementioned correlation. Once these improvements were implemented, a new variable was taken into account for the cloning process, namely volume-surface ratio. Finally, the algorithm was optimized with the aim of optimizing its run time and parallelizing it [29–32]. Furthermore, the algorithm's parameters were calibrated for better results [13].

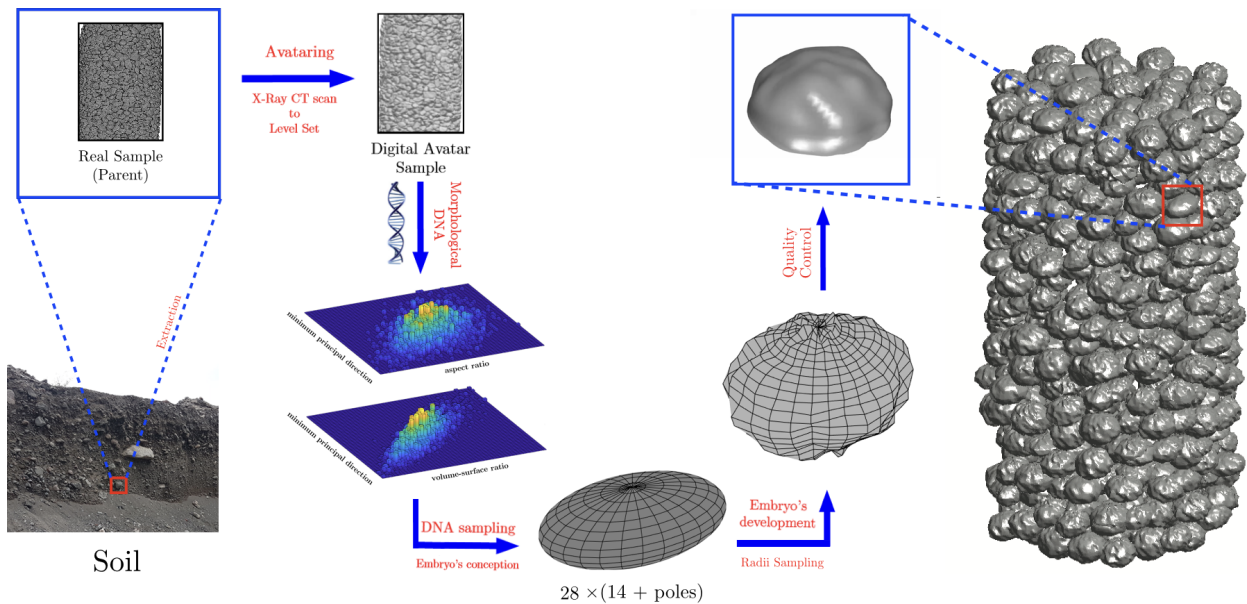


Figure 1: Cloning's process and mechanical test: a small sample of real soil is extracted and then 3DXRCT scanning is performed on it to obtain level set representations of each grain of the real sample. Then, the grains morphological features are extracted (morphological DNA). This DNA is used to generate multivariable probability density distributions from where data is sampled using a multivariable Monte Carlo scheme. Thus, an embryo (equivalent ellipsoid) is generated by sampling from the parents sample morphological DNA and radii distributions. Finally, a quality control is performed and the embryo is included in a pool new cloned grains that is used for simulation by means of a discrete element scheme (3D LS-DEM).

In this work, a soil sample of regolith simulant was scanned using 3D X-ray CT scanning to obtain the level set representation of each grain in the sample. This work was carried on

has been performed in the stages, as shown by Figure 1. First, the morphological DNA from the sample grains (parents) is extracted [13]. Second, a clone's embryo (equivalent ellipsoid) is generated by sampling values from the multivariable aspect ratio and minimum principal direction's distribution. Third, the embryo is developed by means of an enhanced radii sampling scheme that uses a weighted average methodology based on correlations with neighboring surface points. Every embryo is generated based on a spherical mesh and, a radius value sampled from the parents radii distributions is assigned to each mesh point. Then, roundness is matched by sampling a roundness value from the parents distribution and polishing the embryo by means of a laplacian smoother until it reaches the roundness equal to the one sampled from the parents distribution [13]. Finally, a quality control is performed by using the multivariable volume-surface ratio and minimum principal direction distribution obtained from the parents.

To test the first the algorithm, first a pool of 2400 cloned grains is generated and morphological parameters are extracted. Then, a morphological comparison between the clone's morphological parameters and their counterparts obtained from a similar randomly picked pool of parents is conducted. Thus, a second pool of 1000 cloned grains and parents are used to perform a tri-axial test LS-DEM simulation with each pool. These simulations consist of two namely, a hydrostatic phase, and a tri-axial compression from where friction angle mobilization, and axial stress,  $\sigma_1$ , evolution are used as measures of strength and to compare the mechanical response of the clones with respect to the one displayed by the parents. Conclusions are presented as well as observations and directions for further improvements in quality and optimization of the cloning algorithm.

Moreover, note that in this work we use terminology borrowed either from biology or stochastic optimization techniques such genetic algorithm schemes. However, this is not a genetic algorithm where an objective function is optimized by finding either a global maximum or minimum [17]. On the other hand, this algorithm is based on geometric parameters distributions that are Monte Carlo sampled and then combined [13]. Here these morphological parameters are not included as part of any fitness/objective function or set of solutions nor any other parameters used in the process.

## 2 GSC algorithm improvements

In this section we describe a series of improvements that have been implemented to the first algorithm as well as an optimization and parallelization of the original code. First, we address the processing of turning multivariable histograms into multivariable density probability functions, where a Monte Carlo scheme is used to sample from. Then, radii sampling process based on the aforementioned embryo’s spherical mesh. In this regard, an enhanced process is introduced. One of the improvements related to this process has to do with taking into account, for a given mesh point, the radii values of neighboring mesh points. Moreover, an extra final step is added, where a quality control based on volume-surface ratio matching is performed as well as the optimization of some read/write operations are described.

### 2.1 Multivariable distributions

In the first version of this algorithm (GSC 1.0) [13], simple variable distributions of the morphological parameters were considered assuming them to be uncorrelated random variables. Now, in this new version of GSC, correlations among the morphological distributions used in the first version in the embryo’s conception [13], parameters from where multivariable distributions are obtained. The results of these calculations are shown in Table 2.1.

	aspect ratio	roundness	vol.-surf. ratio	min. p. dir.
aspect ratio	1.00	-0.13	0.22	0.51
roundness	-0.13	1.00	0.88	-0.36
volume-surface ratio	0.22	<b>0.88</b>	1.00	-0.34
min. principal direction	<b>0.51</b>	-0.36	-0.34	1.00

Table 1: Morphological parameter’s correlation matrix.

When high enough correlation values in table 2.1 are found, a two-variable parameter histogram is then obtained for those parameters, and by means of (cubic) interpolation, turned into a two-parameter PDF. Thus, from table 2.1, note that there exists a high positive linear correlation of 0.88 between the minimum principal direction and the volume-surface ratio, as expected, and a correlation of 0.51 between the aspect ratio and the minimum principal direction. The value of -0.13 shows that there is no correlation between aspect ratio (a measure of sphericity) (length scale related to order of the grain’s diameter), and the roundness (scale related to the order of the grain’s

diameter divided by 10). This was expected as well, since these two parameters are not related in length scale (“orthogonal”) so a correlation value close to zero (-0.13) gives us confidence about the morphological parameters calculation process. On the other hand, a negative correlation of -0.36 is found between minimum principal direction and roundness. This is also expected since the minimum principal directions are closer in length scale to roundness than the grain’s diameter.

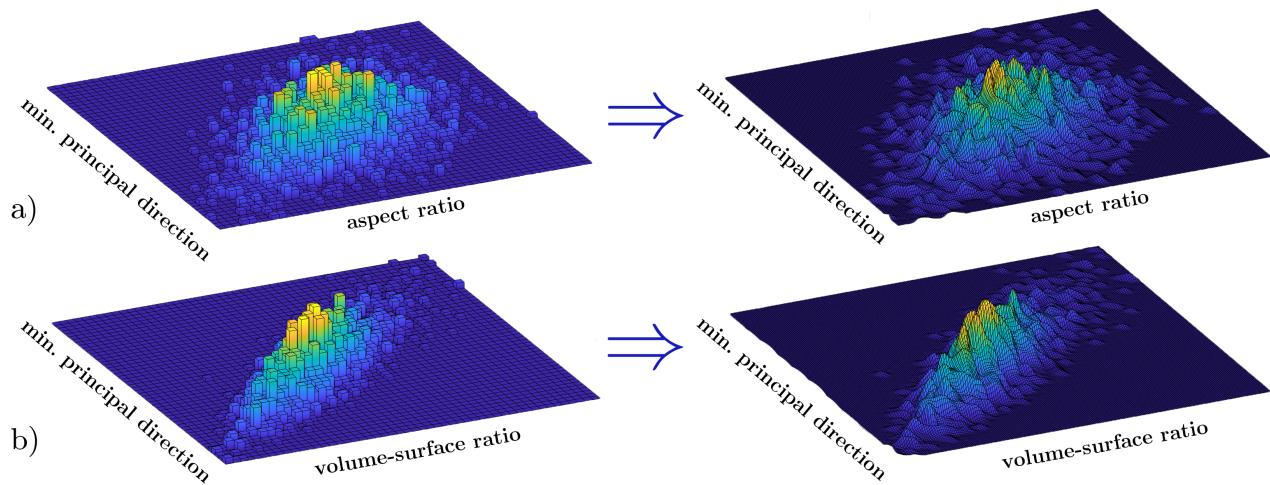


Figure 2: The obtention of multivariable distributions from the morphological DNA. For instance, with two variables (minimum principal direction and volume-surface ratio or aspect ratio) it is possible to generate a two-variable histogram that then, by means of cubic interpolation, is turned into a two-variable probability density function.

As mentioned before, from the correlations in Table 2.1, we generate two-variable histograms for those parameters in which correlation values are “high-enough”. Then, probability density functions are obtained by means of interpolation. For this work, linear, cubic, biharmonic and thin-plate spline interpolation [39] schemes were applied and compared. The best fitting was obtained by using cubic interpolation, which showed a better representation of the histograms. This is illustrated in Figure 2.

## 2.2 Multivariable Monte Carlo method

Once the two-variable probability density functions are obtained from the values of the parents morphological parameters and their corresponding linear correlations, a sampling Monte Carlo (acceptance-rejection) process is used.

### 2.3 Radii sampling

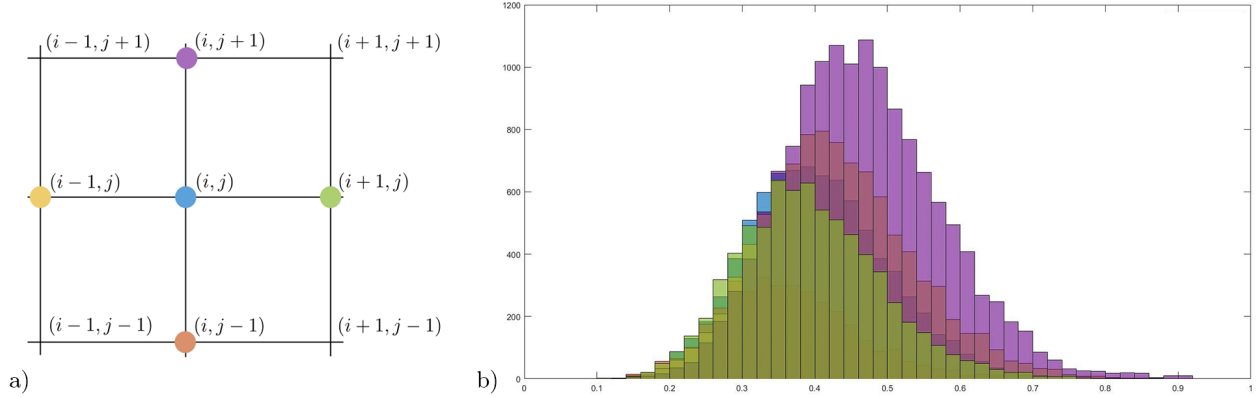


Figure 3: a) For a given mesh point  $(i,j)$  of the embryo's spherical mesh with corresponding radii distribution (figure b) color cyan) obtained from the parent's radii values at the same coordinates than those of the mesh point  $(i,j)$ , and neighboring points on the embryo's spherical. b) Green histogram displays the distribution of radii of regolith simulant for the mesh point  $(i+1,j)$ , blue histogram for the point  $(i,j)$ , purple for  $(i,j+1)$ , orange the point  $(i,j-1)$ , yellow for  $(i-1,j)$  which is on the back.

First, for the spherical radius distributions, all the grains that belong to the sample of parents are aligned with their corresponding principal directions by using a spherical mesh, where the maximum principal direction and minimum principal direction correspond to  $(\Phi = 0, \Theta = \pi/2)$  and  $\Theta = 0$  respectively. [13]. Then, for all the grains, we obtain the radii values of the spherical mesh applied on the parents, so we get a distribution of radii values for each point of this mesh. Radii's distributions corresponding to each mesh point of the spherical mesh applied to each parent were checked for correlation with the distributions of neighbouring mesh points. Figure 3 part b) suggests there is a relation between the points defined in Figure 3 part a). In particular, we analyzed linear correlation between a fixed radius in the mesh and its neighbors and calculated their coefficients. To illustrate it, coefficients for a fixed point are shown in Table 2.3, similar results are obtained for the rest of the mesh points.

Node	$(i,j)$
$(i,j)$	1.00
$(i,j-1)$	0.92
$(i-1,j)$	0.97
$(i,j+1)$	0.86
$(i+1,j)$	0.99

Table 2: Node's correlation for a sampled point in the mesh.



From Figure 3 part b), note that there is a strong linear correlation between a fixed point and its neighbors, so t tests were performed in order to confirm the significance of each correlation coefficient. Results from these tests determined that the correlation coefficients were significant for each point in the mesh 2.3. Therefore, a better method for sampling radius was used (a weighted average) to assign the radii values for each node (i,j) in the ellipsoid’s mesh, taking correlation coefficients as weights. Figure 4 illustrates how the continuity of the radii is improved with this enhanced radii sampling method.

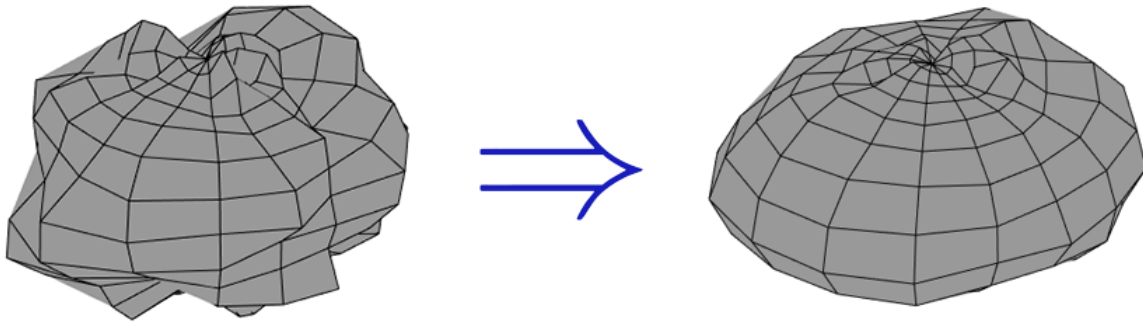


Figure 4: From left to right: an embryo resulting from the radii sampling method of version 1.0, and an embryo resulting from the improved radii sampling, both generated from a pool of 2769 parents.

## 2.4 Quality control

We improved algorithm 1.0 by adding a strict quality control, which uses volume-surface ratio (excluded in the cloning process [13]), and minimum principal direction distribution. After the radii sampling was enhanced, the grain has a minimum principal direction already assigned and a volume-surface ratio is calculated. Then, we use the assigned min. principal direction and randomly sample a value for the volume-surface ratio (by using the Monte Carlo scheme) from the two-variable distribution (see Fig. 2 b) right side) and compare both values of the volume-surface ratio. If the error between the calculated and sampled volume-surface ratio is within 1%, the grain is accepted and saved in a level set function, otherwise, the grain is discarded. This error tolerance is fixed by the user, Figure 5 shows the grain’s acceptance rate as a function of error tolerance using sets of 50 grains.



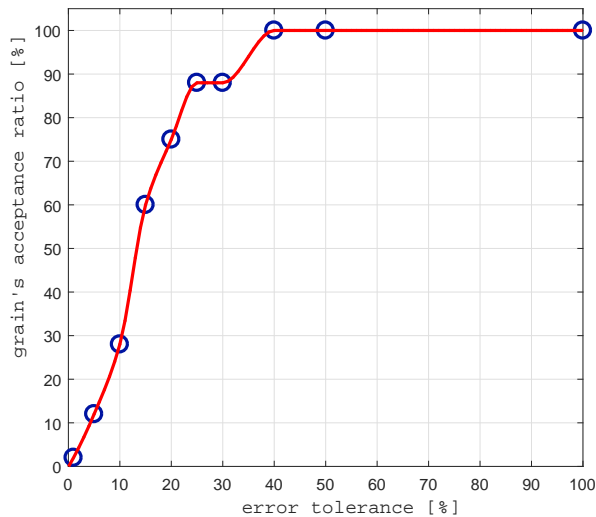


Figure 5: Grain's acceptance rate with respect to error tolerance using sets of 50 grains.

## 2.5 Parallelization and optimization

After the strict quality control is performed most grains are rejected, and in order to replace these missing grains the code was restructured and dynamic vectors were created. These dynamic vectors are used in the cloning process to store information of each clone such as their grain number, aspect ratio, minimum principal direction, roundness, volume-surface ratio and diameter, which are proxies of saved LS files (of the cloned grains) in the hard disk drive (HDD). Moreover, with the two implementations previously mentioned, data access is about 33 times faster since it is stored in the random access memory (RAM) memory instead of the HDD.

All these changes resulted in an average time increment from 45 seconds to 15 minutes in the cloning of one grain. Therefore, a parallelization and optimization of the algorithm was performed, which led to a 75% saving of computational cost. First, we look for the existence of a bottleneck in the three parts of the cloning process [13]. We found that in the last part of the process, the function that assembles the grain could to be calibrated so, we adjusted it's parameters and reduced the total runtime by 25% approximately. Then, other modifications to the algorithm were carried out to parallelize it and reduced the generation time of the clones by 50%.

### 3 Algorithm calibration

Here we describe the parameters of the algorithm that are calibrated, spherical’s mesh and morphological DNA (i.e., aspect ratio, roundness, volume-surface ratio and particle diameter) histogram’s number of bins, mentioned in the knobs section of the first algorithm [13]. In addition, the level set resolution of the clones was increased. Finally, various trials containing different sets of values for these parameters are presented and compared, and the best set is selected using the lowest average error of the morphological DNA as criterion.

In version 1.0, the resolution for the embryo’s spherical mesh was set to 16 azimuthal zones and 8 polar zones. According to the best set of parameters, in this version, we use 28 azimuthal zones and 18 polar zones, which yield a higher resolution (see Fig. 6), hence a lower error in the generation of the grains [33]. Furthermore, for a better representation of grains’ irregular shapes, the resolution of the level set was increased from to  $30 \times 30 \times 30$  [13] (see Fig. 7 part a)) to a resolution of  $45 \times 45 \times 45$  (see Fig. 7 part b)).

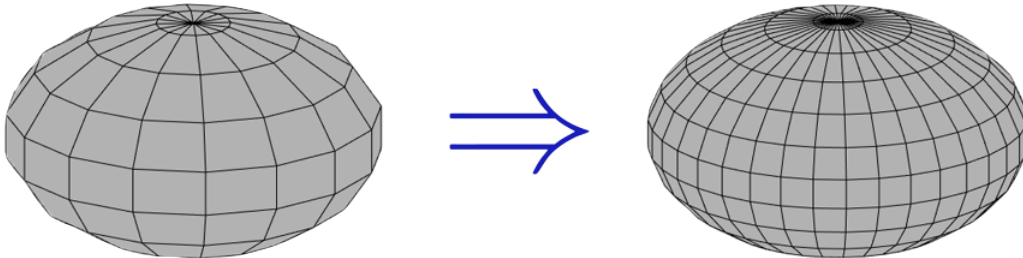


Figure 6: Embryo’s higher spherical mesh resolution. Left: spherical mesh of  $16 \times (8 + \text{poles})$ . Right: spherical mesh of  $28 \times (18 + \text{poles})$ .

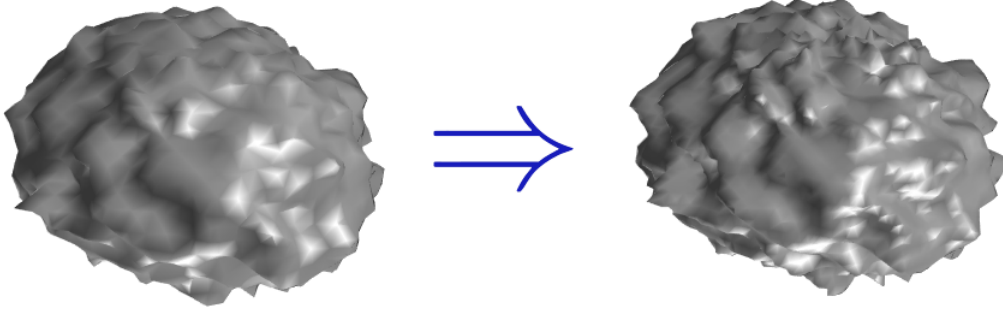


Figure 7: Left: grain’s level set grid made of  $30 \times 30 \times 30$  points. Right: same grain with a level set grid of  $45 \times 45 \times 45$ .

We set trial configurations using embryos’ spherical mesh resolution and histogram’s number of bins, which are going to be compared under the criteria of lowest average error with respect to the morphological DNA (see subsection 4.1). First, the mesh’s resolution values range from  $28 \times (14 + 2)$  to  $34 \times (24 + 2)$ . Note that, the number two in the addition operation of this mesh’s resolution, corresponds to the number of poles of the spherical mesh. Second, the number of bins used for the morphological DNA sampling are 50 and 60. Finally, fixed values of the parameters for this version (2.0) are highlighted in red in Table 3.

Parameters	Trial				
	1	2	3	4	5
embryo’s mesh	$28 \times (14 + 2)$	$30 \times (15 + 2)$	$30 \times (15 + 2)$	$28 \times (18 + 2)$	$34 \times (24 + 2)$
number of bins	50	50	60	50	50

Table 3: Parameters of the different versions of the algorithm used in the calibration

## 4 Morphological matching

We evaluate the main morphological DNA, i.e, aspect ratio, roundness, principal geometric directions, and spherical radius, of the cloned grains with respect to the ones obtained from their original counterparts, for this matter, the samples of parents and clones used contain 2400 grains each.

First, we compare the aspect ratio distribution of parents and clones, and from Figure 8 we conclude that both have very similar distributions with slight greater values of aspect ratio for the clones. However, note that the mean of the clones distribution is off with respect to the mean of the parents distribution with an error of 5.64%, while the standard deviation of the clones distribution

has an error of 10.17% with respect to its counterpart.

Second, the roundness distributions have a mean error of 5.16%, and the standard deviation of the clone's distribution has an error of 13.35% with respect to the parents. Clones still display lower roundness values (see Fig. 9), which were discussed in the first version of the algorithm [13]. Even, if its standard deviation is affected by the reduced roundness, it is similar to the parents deviation.

Third, we obtained the distributions for the grain diameter and obtained an error of 10.41% in the mean, and 38.69% in the standard deviation between the clone's and their parents. The bias shown in Figure 10 with smaller grain diameters could be due to the selection of a minimum principal direction to generate the embryo. To overcome this problem a quality control could be implemented using the grain's diameter and volume-surface ratio. This is not included in this version but, it is mentioned in section 8. In addition, parents exhibit a coefficient of uniformity  $C_u = D_{60}/D_{10} = 1.26$  and a coefficient of curvature  $C_c = D_{30}/(D_{60} \times D_{10}) = 0.76$ , similar coefficients are given by the clones  $C_u = 1.15$  and  $C_c = 0.79$ , where  $D_{10}, D_{30}, D_{60}$  are grain's diameters with 10% , 30% and 60% passing, respectively. The  $C_u$  coefficient gives an error of 8.29% and the error of  $C_c$  is 4.28% (see Figure 12) where  $D_{10}$  and  $D_{30}$  are similar but,  $D_{60}$  has a bigger difference.

Finally, the volume-surface ratio distributions have a mean error of 2.42%, and a standard deviation of 30.12% when comparing parents and clones. There is less standard deviation, and thus, variance in the values of aspect ratio of the clones than their parents but, their means are very similar (see Figure 11). Note that, the addition of the quality control of 1% is directly reflected in lower errors of the mean and standard deviation of volume-surface ratio with respect to the first version. [13].

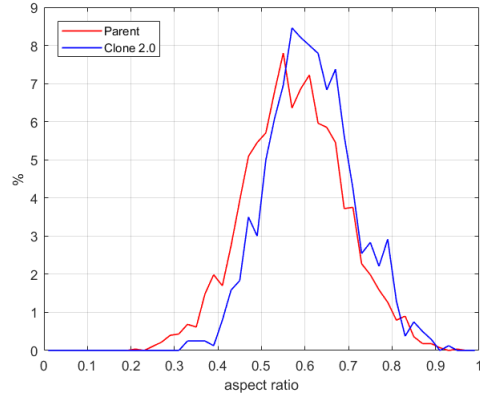


Figure 8: Aspect ratio distributions calculated for the clones and parents

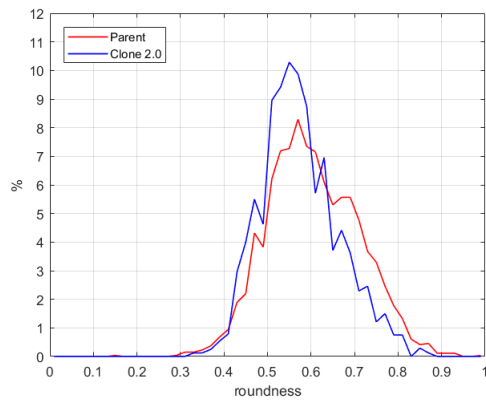


Figure 9: Roundness distributions obtained from parents and clones

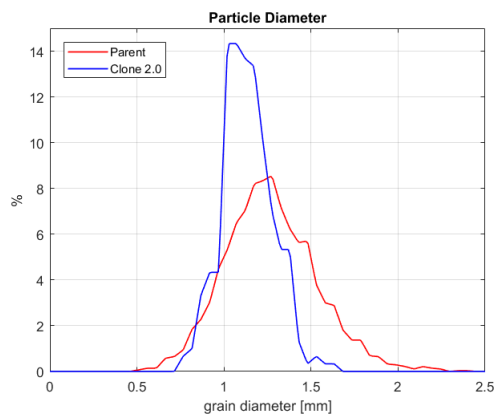


Figure 10: Grain's diameter distribution calculated for the clones and parents

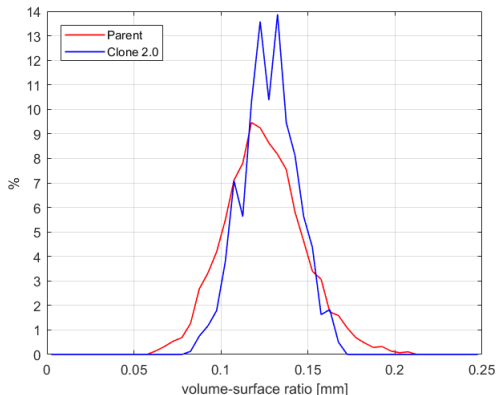


Figure 11: Volume to surface ratio computed for parents and clones

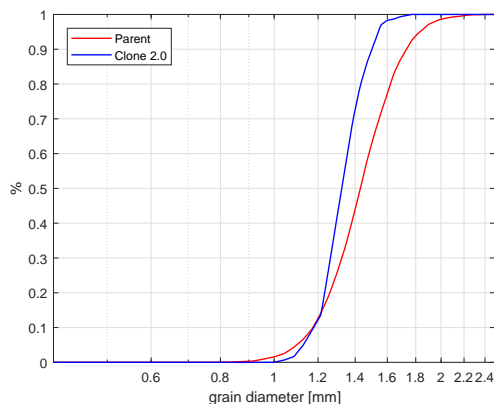


Figure 12: percentage of grains passing versus log of grain's diameter corresponding to last figure

#### 4.1 Errors

In this subsection we compare the errors in the mean and standard deviation for the clones of the first algorithm and trial configurations of clones in this version of the algorithm with respect to their parents. For this matter, we generated 2400 clones from the pool of 2769 regolith simulant (parent grains), and sampled a pool of 2400 parents. We calculated errors (in percentage) from the algorithm 1.0 and the trials in section 3 to compare their mean and standard deviation displayed in tables 4 and 5 respectively.

Morphological Parameter	Trials					
	<i>0</i>	<i>1</i>	<i>2</i>	<i>3</i>	<i>4</i>	<i>5</i>
Aspect ratio	10.95	7.38	7.28	9.22	5.64	5.23
Grain diameter	0.58	10.09	10.53	10.37	10.41	9.18
Roundness	2.20	4.21	6.18	8.05	5.16	6.56
Volume-surface ratio	34.84	6.32	27.69	4.59	2.42	5.06
<b>Average error</b>	<b>12.14</b>	<b>7.00</b>	<b>12.92</b>	<b>8.06</b>	<b>5.91</b>	<b>6.51</b>

Table 4: Mean error in percentage for each version of the algorithm and each morphological property

Morphological Parameter	Trials					
	<i>0</i>	<i>1</i>	<i>2</i>	<i>3</i>	<i>4</i>	<i>5</i>
Aspect ratio	6.36	15.66	6.79	17.63	10.17	16.21
Grain diameter	20.68	40.3	40.26	39.55	38.69	41.80
Roundness	9.44	14.38	7.61	23.56	13.35	18.95
Volume-surface ratio	57.45	28.79	60.71	32.15	30.12	35.23
<b>Average error</b>	<b>23.48</b>	<b>24.78</b>	<b>28.84</b>	<b>28.22</b>	<b>23.08</b>	<b>28.05</b>

Table 5: Standard deviation error in percentage for each version of the algorithm and each morphological property.

The error in the means show that for aspect ratio and volume-surface ratio errors were reduced while the grain’s diameter and roundness increased (see Table 4). On the other hand, error in standard deviations for volume-to surface ratio decreased but, aspect ratio, grains diameter and roundness errors increased. In sum, we have that the algorithm version with less average error is 2.0 using trial 4 with an embryo’s mesh of  $28 \times (18 + 2)$  and a level set resolution of  $45 \times 45 \times 45$  using 50 histogram bins. Comparing both versions we obtain about 6% less error in the means and 0.40% less error in the standard deviation than the first version of the algorithm.

## 4.2 Results

We ran the algorithm in Matlab 2017a with parallel pool [29] using 18 computers, with specific characteristics (see Table 6), in a laboratory of Universidad San Francisco de Quito. As a result 3554 clones were generated from a pool of 2769 parents and the average time taken to generate each cloned grain was 5 minutes. From these grains, we take 5 regolith simulant parents and cloned grains obtained from version 2.0 shown in Figure 13,

<b>Operative System</b>	Windows 10 Pro x 64
<b>Processor</b>	i5-3570 @3.40 GHz
<b>RAM</b>	8 GB
<b>ROM</b>	500 GB

Table 6: Technical characteristics of the computers used to generate a clones sample of 3554.

The code takes advantage of all the physical cores of the processor, in our case, the job is divided into the 4 available cores in the laboratory computers. This job scheduling is synchronous [30–32], in other words, if a batch of four grains or less are assigned to the four available cores, the batch's generation ends after each core clone their respective grain, then, another batch is processed until all the job is done.

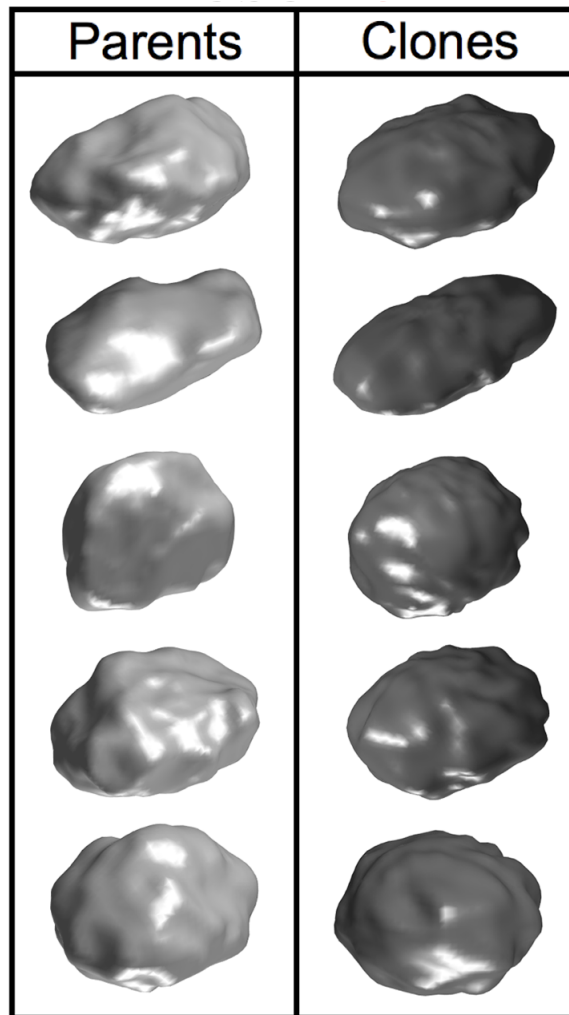


Figure 13: Five random sampled regolith simulant parents and clones for visual inspection and comparison.



## 5 Mechanical matching

In this section, we compare the soil’s mechanical behavior of regolith simulant parents and clones. The clones produced by the geometry-based stochastic algorithm were included in simulations using level set (LS) discrete element method scheme (3D LS-DEM) of a tri-axial test [20], which have shown to reproduce qualitatively and quantitatively macroscopic behavior of grains. These simulations consist of two namely, a hydrostatic phase, and a tri-axial compression from where friction angle mobilization, and axial stress  $\sigma_1$ , evolution are used as measures of strength and to compare the mechanical response of the clones with respect to the parents.

<b>Membrane Parameter</b>	<b>Value</b>	<b>Units</b>
Sphere radius	0.15	mm
Diameter	10	mm
Normal bond stiffness	100	N/m
Shear bond stiffness	100	N/m
Normal stiffness	$3.0 \times 10^4$	N/m
Shear stiffness	0	N/m

Table 7: Values of parameters used in simulation of membrane used in the tri-axial tests for the parents and clones

The simulations were performed on Mode Mat’s cluster Quinde using 32 cores, the samples of cloned and real grains for each simulation contained 1000 grains, 567 membrane particles for the parents and 522 membrane particles for the clones, the parameters of the membrane are displayed in Table 8. Then, differences in percentage for each parameter of the samples are calculated and displayed in table 9. The hydrostatic compression took 18 hours for the parents and 141 hours for the clones, and the result of this compression is shown in Figure 14. In addition, the tri-axial test with 20% deformation was done in 17 hours for both, the parents and clones, and the resultant configuration is shown in Figure 16.

<b>Initial Conditions</b>	<b>Parents</b>	<b>Clones</b>
Prescribed hydrostatic pressure	5.1	5.1
Actual hydrostatic pressure	4.11	4.03
Height	454.22	464.74
Height-diameter ratio	2.11	2.01
Porosity	32.7	33.4

Table 8: Parents and clones tri-axial test initial conditions after isotropic compression.

Initial Conditions	Error [%]
Actual hydrostatic pressure	1.95
Height	2.32
Height-diameter ratio	4.98
Porosity	2.14

Table 9: Error in the tri-axial test initial conditions of clones with respect to parents after isotropic compression.

The sample of digitalized parents are packed and ready to be hydro-statically compressed but, the clones presented a challenge because they needed to be packed first. In order to solve this problem, we generated positions for the cloned grains in the packing by using spheres with the maximum value of radius of the grains in the pool and a minimum distance between them. Additionally, more than a thousand simulations failed because the grains were too far from each other or superposed, which led to the tearing of the membrane.

As can be seen from Table 8, for the LS-DEM simulations we prescribe an hydrostatic confinement pressure of 5.1 [ $F/L^2$ ]. Moreover, a stress tensor  $\sigma$  can be decomposed into the sum of its volumetric  $p\mathbf{1}$  and deviatoric  $\mathbf{s}$  parts [34].  $\sigma = p\mathbf{1} + \mathbf{s}$ , where  $p = tr(\sigma)/3$  is the mean normal stress, and  $\mathbf{1}$  is the  $3 \times 3$  identity. The second invariant  $J_2$  is defined as  $J_2 = (\mathbf{s} : \mathbf{s})/2$ . Thus, for the parents we have

$$\sigma = \begin{pmatrix} 3.39 & 0 & 0 \\ 0 & 3.46 & 0 \\ 0 & 0 & 5.49 \end{pmatrix} \quad p\mathbf{1} = 4.11 \cdot \mathbf{1} \quad \mathbf{s} = \begin{pmatrix} -0.72 & 0 & 0 \\ 0 & -0.65 & 0 \\ 0 & 0 & 1.37 \end{pmatrix}$$

with  $J_2 = 1.41$ . On the other hand, for the clones

$$\sigma = \begin{pmatrix} 4.78 & 0 & 0 \\ 0 & 3.74 & 0 \\ 0 & 0 & 3.56 \end{pmatrix} \quad p\mathbf{1} = 4.03 \cdot \mathbf{1} \quad \mathbf{s} = \begin{pmatrix} 0.76 & 0 & 0 \\ 0 & -0.29 & 0 \\ 0 & 0 & -0.47 \end{pmatrix}$$

so clones corresponding second invariant is  $J_2 = 0.44$ .

The results of the second invariant,  $J_2$ , show that packing of parents have a bigger deviator strain than the packing of clones. This is due to the small size of the samples (1000 grains each), but as the size increases the actual pressure will converge to the applied pressure.

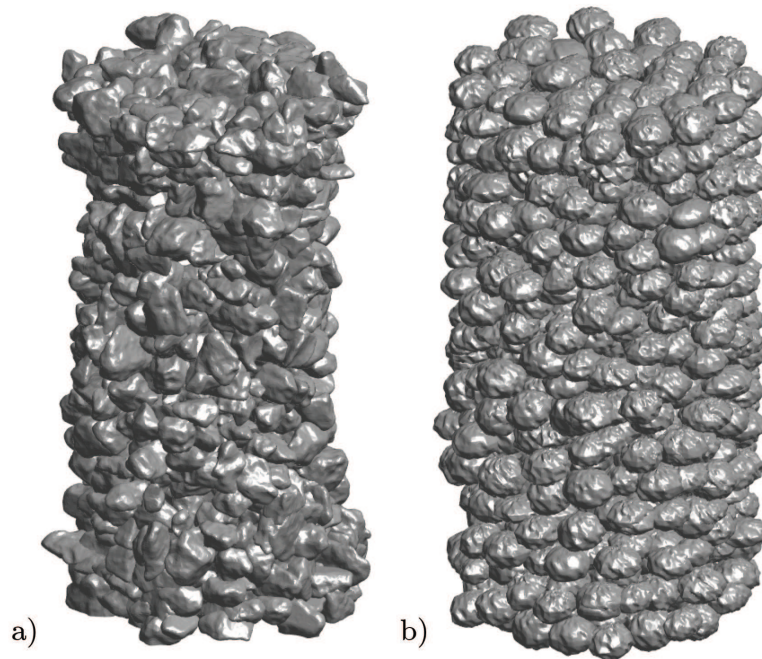


Figure 14: Samples of 1000 grains after hydrostatic compression of a) parents b) clones.

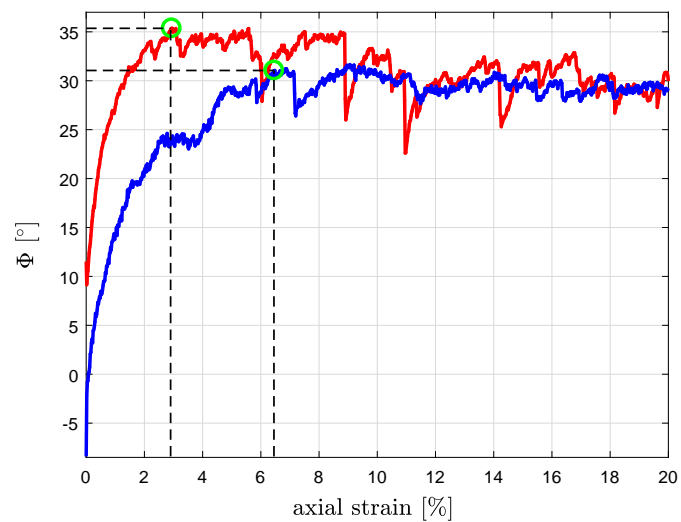


Figure 15: Friction angle mobilization versus axial strain from the samples of parents and clones made of 1000 grains each, and undergoing tri-axial compression. Here, red line corresponds to parents and blue line to clones.

	friction angle [°]	strain [%]	$\sigma_1 [F/L^2]$
parents	35.36	2.90	13.28
clones	31.05	6.45	14.81
error	12.11%	122.41%	11.52%

Table 10: Tri-axial test results for parents and clones with samples of 1000 grains each. In this table, the error has been computed for each parameter and with respect to the parents results.

From the results obtained after performing the tri-axial simulations using 3D LS-DEM scheme, we see that parents and clones have similar mechanical behavior (see Fig. Figure 15). To compare these results, we use Table 5, which show that the peak friction angle for the clones is similar to their parents and the axial pressure values corresponding to the maximum strain are identical although the strain is not the same. The final configuration of the packings of parents and clones are shown in Figure 16. Recall that, this mechanical comparison included 1000 grains parents and clones each, we expect the clones' behavior to be very similar to its parents as the size of the samples increases.

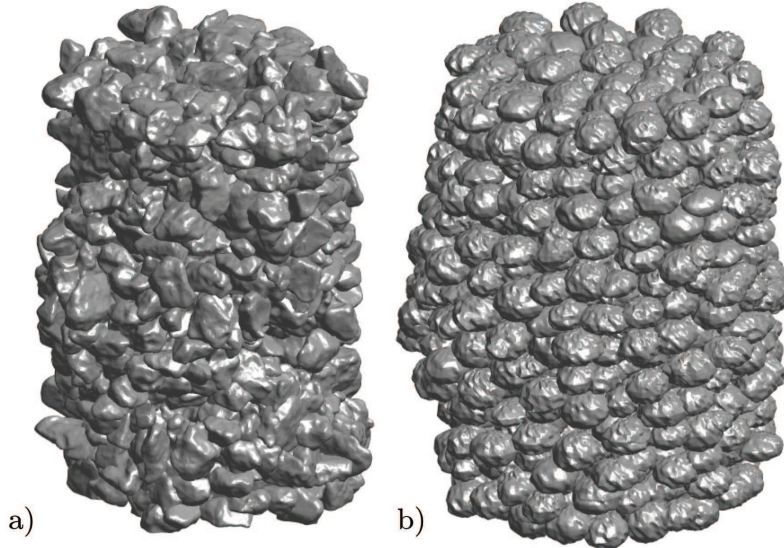


Figure 16: Final configuration after the tri-axial compression tests have finished with a total axial deformation of 20% a) parents and b) clones.

## 6 Further improvements

One of the main novelties of GSC is that it can be coded under the objects oriented paradigm which makes it reusable, more simple and efficient than procedural programming [35–38]. More importantly, it can be generalized to “clone” not only grains but any three-dimensional object.

The code can be restructured to reduce algorithm’s execution time. The algorithm reads and writes repeatedly data stored in the hard disk drive, which results into a slowdown of the process. This data can be read once and loaded in the RAM memory, and then saved only when the algorithm finishes the cloning process. This will also reduce errors in the generation of the clones since the roundness matching process (described in [13]) is performed after each batch of clones comply the quality control.

The generation of grains can be parallelized to reduce algorithm’s execution time, specially when the number of grains approximate 10000 or more grains. The program can be fully parallelized so one core generates one grain, thus taking advantage of all the cores and threads. This might reduce the execution time dramatically if for instance CUDA is used.

Moreover, the calibration of the embryo’s mesh can be automated to reduce algorithm’s execution time and minimize error. In this version, the calibration is manual but, this task can be coded so the user doesn’t need to calibrate it.

In the present version of the algorithm, there is a bias in the grains’ diameter where the values obtained from the clones are lower than the parents. Therefore, an additional quality control can be included using volume-surface ratio and grain’s diameter to improve the matching for the distributions of this last feature.

Furthermore, the number of points sampled can be optimized to reduce algorithm’s execution time. The algorithm samples a set of points that form a neighborhood for each radius instead, we can sample a set of points for all the mesh and then use them in the development of the embryo to reduce the number of calculations.

All functions and operations can be checked if they can be performed in other ways to reduce algorithm’s execution time. For instance the change of coordinates system could have other functions which could reduce time.

## 7 Conclusions

We developed a computational algorithm that was used to “clone” an arbitrary number of grains using grain morphologies of a real sample of digitalized grains. These grains not only satisfied their parents morphological features, but they also showed a similar mechanical behavior after clones and their parents were included into a numerical DEM simulation.

This version of the algorithm is based on the geometry or morphological DNA of the parent grains and relies on its multivariable statistical distributions (aspect ratio, minimum principal direction, roundness and volume-surface ratio). After all the morphological DNA is extracted from the real sample that has been digitalized, the algorithm generates a clone’s embryo (equivalent ellipsoid), by sampling values of aspect ratio and minimum principal direction from its two-variable distribution by using a multivariable Monte Carlo scheme. Then, the embryo is developed by sampling radius in an enhanced radii sampling process. Next, the developed embryos’s roundness is matched with their parents sampled value by polishing them with a laplacian smoother. Finally, a quality control is carried out using volume-surface ratio and minimum principal direction multivariable distribution.

After that, the algorithm was used to generate a pool of 2400 clones and calculations were performed to obtain the morphological DNA. The distributions of morphological DNA these clones were compared with respect to the ones acquired from a pool of the same size of random picked parents (see Figures 8, 9, 11, 10 and 12), from where we infer that the clones morphologically match much more accurately their parents in this second version.

Additionally, A packing of 1000 parents was included in a tri-axial LS-DEM simulation and a similar packing of clones was generated with the same number of grains, both had with an initial deviator strain different from zero. The results from the simulation show a similar behavior in terms of friction angle,  $\sigma_1$  and peak strain. Finally, the algorithm future improvements are analyzed and described in section 8.

## 8 Acknowledgements

This research was carried out using the research computing facilities and advisory services offered by Scientific Computing Laboratory of the Research Center on Mathematical Modeling: MODEMAT, Escuela Politécnica Nacional -Quito.

## References

- [1] Cundall, P.A., Strack (1979). O.D.L.: A discrete numerical model for granular assemblies. *Geotechnique*, 29, 4765.  
<https://doi.org/10.1680/geot.1979.29.1.47>
- [2] Cundall, P.A. and Hart R. (1972). Numerical Modeling of Discontinua. *Engineering Computations*, 9(2), pp.101-113.  
<https://doi.org/10.1108/eb023851>
- [3] Cundall, P.A. and Hart R., (1971). A computer model for simulating progressive, large scale movements in blocky rock systems. *Proceedings of the International symposium Rock Fracture, ISRM, Nancy, II-8*, vol 2.
- [4] Seyed Hosseininia, E. (2012). Investigating the micromechanical evolutions within inherently anisotropic granular materials using discrete element method. *Granular Matter*, 14(4), pp.483-503.  
[https://doi.org/10.1016/0148-9062\(88\)92293-0](https://doi.org/10.1016/0148-9062(88)92293-0)
- [5] Barla, G., Einstein, H. and Kovari, K., (2012). Manuscripts Using Numerical Discrete Element Methods. *Rock Mechanics and Rock Engineering*, 46(4), pp.655-655.  
<https://doi.org/10.1007/s00603-013-0442-3>
- [6] Lu, J., Zhang, C. and Jian, P. (2016). Meso-Structure Parameters of Discrete Element Method of Sand Pebble Surrounding Rock Particles in Different Dense Degrees. *Springer Proceedings in Physics*, pp.871-879.  
[https://doi.org/10.1007/978-981-10-1926-5\\_91](https://doi.org/10.1007/978-981-10-1926-5_91)
- [7] Huang, X., OSullivan, C., Hanley, K. and Kwok, C. (2014). Capturing the state-dependent nature of soil response using DEM. *Geomechanics from Micro to Macro*, pp.61-65.  
<https://doi.org/10.1201/b17395-10>
- [8] Cundall, P. (1988). Formulation of a three-dimensional distinct element modelPart I. A scheme to detect and represent contacts in a system composed of many polyhedral blocks. *International*



- Journal of Rock Mechanics and Mining Sciences & Geomechanics Abstracts*, 25(3), pp.107-116.  
[https://doi.org/10.1016/0148-9062\(88\)92293-0](https://doi.org/10.1016/0148-9062(88)92293-0)
- [9] Khalili, M., Brisard, S., Bornert, M., Aimedieu, P., Pereira, J. and Roux, J. (2017). Discrete Digital Projections Correlation: A Reconstruction-Free Method to Quantify Local Kinematics in Granular Media by X-ray Tomography. *Experimental Mechanics*, 57(6), pp.819-830.  
<https://doi.org/10.1007/s11340-017-0263-5>
- [10] Kim, K., Zhuang, L., Yang, H., Kim, H. and Min, K. (2015). Strength Anisotropy of Berea Sandstone: Results of X-Ray Computed Tomography, Compression Tests, and Discrete Modeling. *Rock Mechanics and Rock Engineering*, 49(4), pp.1201-1210.  
<https://doi.org/10.1007/s00603-015-0820-0>
- [11] Fu, X., Dutt, M., Bentham, A., Hancock, B., Cameron, R. and Elliott, J. (2006). Investigation of particle packing in model pharmaceutical powders using X-ray microtomography and discrete element method. *Powder Technology*, 167(3), pp.134-140.  
<https://doi.org/10.1016/j.powtec.2006.06.011>
- [12] Wang, L., Park, J. and Fu, Y. (2007). Representation of real particles for DEM simulation using X-ray tomography. *Construction and Building Materials*, 21(2), pp.338-346.  
<https://doi.org/10.1016/j.conbuildmat.2005.08.013>
- [13] Jerves, A., Kawamoto, R., & Andrade, J. (2017). A geometry-based algorithm for cloning real grains. *Granular Matter*, 19(2).  
<http://dx.doi.org/10.1007/s10035-017-0716-7>
- [14] Jerves, A., Kawamoto, R., & Andrade, J. (2015). Effects of grain morphology on critical state: a computational analysis. *Acta Geotechnica*, 11(3), pp.493-503.  
<http://dx.doi.org/10.1007/s11440-015-0422-8>
- [15] Kawamoto, R., And, E., Viggiani, G. and Andrade, J. (2018). All you need is shape: Predicting shear banding in sand with LS-DEM. *Journal of the Mechanics and Physics of Solids*, 111, pp.375-392.  
<http://dx.doi.org/10.1007/s11440-015-0405-9>

- [16] Vlahini, I., Kawamoto, R., And, E., Viggiani, G. and Andrade, J. (2016). From computed tomography to mechanics of granular materials via level set bridge. *Acta Geotechnica*, 12(1), pp.85-95.  
<http://dx.doi.org/10.1007/s11440-016-0491-3>
- [17] Borrelli, F., Bemporad, A. and Morari, M. (2003). *Geometric Algorithm for Multiparametric Linear Programming*. *Journal of Optimization Theory and Applications*, 118(3), pp.515-540.  
<https://doi.org/10.1023/B:JOTA.0000004869.66331.5c>
- [18] Robert, C. (2016). Monte Carlo Methods. *Wiley Statsref: Statistics Reference Online*, 1-13.  
<http://dx.doi.org/10.1002/9781118445112.stat03876.pub2>
- [19] Glasserman, P. (2010). Generating Random Numbers and Random Variables. *Monte Carlo methods in financial engineering*. New York: Springer.
- [20] Kawamoto, R., And, E., Viggiani, G., & Andrade, J. (2016). *Level set discrete element method for three-dimensional computations with triaxial case study*.  
<http://dx.doi.org/10.1016/j.jmps.2016.02.021>
- [21] Kawamoto, R., And, E., Viggiani, G., & Andrade, J. (2018). All you need is shape: Predicting shear banding in sand with LS-DEM. *Journal Of The Mechanics And Physics Of Solids*.  
<http://dx.doi.org/10.1016/j.jmps.2017.10.003>
- [22] Lim, K. and Andrade, J. (2013). Granular element method for three-dimensional discrete element calculations. *International Journal for Numerical and Analytical Methods in Geomechanics*, 38(2), pp.167-188.  
<http://10.1002/nag.2203>
- [23] Mollon, G. and Zhao, J. (2014). 3D generation of realistic granular samples based on random fields theory and Fourier shape descriptors. *Computer Methods in Applied Mechanics and Engineering*, 279, pp.46-65.  
<http://10.1016/j.cma.2014.06.022>
- [24] Jin, C., Yang, X. and You, Z. (2015). Automated real aggregate modelling approach in discrete element method based on X-ray computed tomography images. *International Journal of*

*Pavement Engineering*

<http://dx.doi.org/10.1080/10298436.2015.1066006>

- [25] Lim, K. and Andrade, J. (2015). Discrete modeling of granular media: a NURBS-based approach.  
[https://thesis.library.caltech.edu/8734/61/lim\\_kengwit\\_2015\\_thesis.pdf](https://thesis.library.caltech.edu/8734/61/lim_kengwit_2015_thesis.pdf)
- [26] ASTM, (1992). Standard Guide for Computed Tomography (CT) Imaging, ASTM Designation E 1441 - 92a. In: 1992 Annual Book of ASTM Standards, Section 3 Metals Test Methods and Analytical Procedures. *ASTM, Philadelphia*, pp. 690-713.
- [27] Ketcham, R.A. and Carlson, W.D., (2001). Acquisition, optimization and interpretation of X-ray computed tomographic imagery: Applications to the geosciences. *Computers and Geosciences*, 27, 381-400.
- [28] Andrade, J. E., Lim, K., Avila, C. F., & Vlahini, I. (2012). Granular element method for computational particle mechanics. *Computer Methods in Applied Mechanics and Engineering*, 241-244, 262-274.  
<https://doi.org/10.1016/j.cma.2012.06.012>
- [29] Mathworks.com. (2017). Parallel Computing Toolbox - MATLAB [online]. Available at:  
<https://www.mathworks.com/products/parallel-computing.html>
- [30] Jung, G., Gnanasambandam, N., & Mukherjee, T. (2012). Synchronous Parallel Processing of Big-Data Analytics Services to Optimize Performance in Federated Clouds. *2012 IEEE Fifth International Conference On Cloud Computing*.  
 Available at:  
<http://dx.doi.org/10.1109/cloud.2012.108>
- [31] Bertsekas, D., & Castanon, D. (1991). Parallel synchronous and asynchronous implementations of the auction algorithm. *Parallel Computing*, 17(6-7), 707-732.  
 Available at:  
[http://dx.doi.org/10.1016/s0167-8191\(05\)80062-6](http://dx.doi.org/10.1016/s0167-8191(05)80062-6)

- [32] Alba, E., & Troya, J. (2001). Analyzing synchronous and asynchronous parallel distributed genetic algorithms. *Future Generation Computer Systems*, 17(4), 451-465..  
Available at:  
[http://dx.doi.org/10.1016/s0167-739x\(99\)00129-6](http://dx.doi.org/10.1016/s0167-739x(99)00129-6)
- [33] Hussaini, M., Leer, B., & Van Rosendale, J. (1997). *Upwind and high-resolution schemes* (p. 303). Berlin: Springer.
- [34] Borja, R. (2013). J2 Plasticity. *Plasticity*, pp.31-58. Berlin: Springer.  
Available at:  
[https://doi.org/10.1007/978-3-642-38547-6\\_3](https://doi.org/10.1007/978-3-642-38547-6_3)
- [35] Brainerd W.S. (2015) Object-Oriented Programming. In: Guide to Fortran 2008 Programming. Springer, London  
Available at:  
[https://doi.org/10.1007/978-1-4471-6759-4\\_12](https://doi.org/10.1007/978-1-4471-6759-4_12)
- [36] Dovey J., Furrow A. (2012). Object-Oriented Programming. In: Beginning Objective-C. Apress, Berkeley, CA  
Available at:  
[https://doi.org/10.1007/978-1-4302-4369-4\\_2](https://doi.org/10.1007/978-1-4302-4369-4_2)
- [37] Craig I. (2007). Object-Oriented Programming Languages: Interpretation  
Available at:  
<https://doi.org/10.1007/978-1-84628-774-9>
- [38] Poo, D., Kiong, D. and Ashok, S. (2008). Object-Oriented Programming and Java.  
Available at:  
<https://doi.org/10.1007/978-1-84628-963-7>
- [39] La.mathworks.com. (2018). *Interpolation Methods- MATLAB & Simulink- MathWorks America Latina*. [online]  
Available at:

<https://la.mathworks.com/help/curvefit/interpolation-methods.html> [Accessed 12 Apr. 2018].